Reprint Series
16 December 1994, Volume 266, pp. 1870–1874

SCIENCE

Toxic Shock Syndrome Toxin–1 Complexed with a Class II Major Histocompatibility Molecule HLA-DR1

Jongsun Kim, Robert G. Urban, Jack L. Strominger, and Don C. Wiley*

Toxic Shock Syndrome Toxin–1 Complexed with a Class II Major Histocompatibility Molecule HLA-DR1

Jongsun Kim, Robert G. Urban, Jack L. Strominger, Don C. Wiley*

The three-dimensional structure of a *Staphylococcus aureus* superantigen, toxic shock syndrome toxin–1 (TSST-1), complexed with a human class II major histocompatibility molecule (DR1), was determined by x-ray crystallography. The TSST-1 binding site on DR1 overlaps that of the superantigen *S. aureus* enterotoxin B (SEB), but the two binding modes differ. Whereas SEB binds primarily off one edge of the peptide binding site of DR1, TSST-1 extends over almost one-half of the binding site and contacts both the flanking α helices of the histocompatibility antigen and the bound peptide. This difference suggests that the T cell receptor (TCR) would bind to TSST-1:DR1 very differently than to DR1:peptide or SEB:DR1. It also suggests that TSST-1 binding may be dependent on the peptide, though less so than TCR binding, providing a possible explanation for the inability of TSST-1 to competitively block SEB binding to all DR1 molecules on cells (even though the binding sites of TSST-1 and SEB on DR1 overlap almost completely) and suggesting the possibility that T cell activation by superantigen could be directed by peptide antigen.

Toxic shock syndrome toxin–1 (TSST-1) is a 22-kD protein superantigen secreted by *S. aureus* that causes toxic shock in humans probably by polyclonal activation and lymphokine secretion from T cells (*1*). Patients exhibit selective expansion of T cells (up to 50% of the total) expressing the $V_\beta 2$ family of TCR β chains (*2*). Like other bacterial and viral superantigens, TSST-1 cross-links the class II major histocompatibility complex (MHC) proteins of antigen-presenting cells to the V_β chains of the antigen receptor of T cells (*3*). Earlier studies indicate that superantigens bind primarily outside of the peptide-antigen binding groove of class II MHC molecules and to mainly conserved regions of TCRs, including a fourth region of hypervariability (CDR4) on V_β chains (*2, 4*). Furthermore, bacterial superantigens function as intact molecules, unlike conventional antigens, which are degraded to a short peptide and complexed with an MHC molecule for recognition by T cells (*5*). Their binding mode may circumvent the clonal specificity of T cells by binding away from the six major TCR hypervariable loops, enabling superantigens to activate a large fraction of all T cells (10 to 30%, hence their name) that bear certain families of TCR V_β chains (*6*).

The x-ray crystal structure of a complex between the superantigen *S. aureus* enterotoxin B (SEB) and the human class II MHC molecule HLA-DR1 was determined recently (*7*). It revealed that SEB binds exclusively to the α chain of DR1 off one edge of the peptide binding groove. One loop of SEB covers residues of DR1 recognized by the TCR during conventional antigen recognition (*8*), which suggests an unconventional model for the interaction between the TCR and MHC during superantigen activation (*7*). Although they are only 16% identical in sequence (*9*), TSST-1 and SEB have very similar three-dimensional structures (*9, 10*). However, sequence differences in TSST-1 at residues corresponding to SEB residues involved in binding to DR1 suggest the existence of substantially different superantigen-DR1 interactions (*7*), although mutation and competition studies suggest substantial overlap in the binding site on DR1 (*11–15*).

Here, we determined the three-dimensional structure of the TSST-1:DR1 complex by x-ray crystallography. The locations of the DR1 and TSST-1 molecules in a crystal of the TSST-1:DR1 complex were both determined by two independent methods with the use of coordinates of the individual molecules (*9, 16*). First, their locations were each found by separate, six-dimensional searches of α carbon models (*17*) through a single isomorphous re-

Table 1. Data processing and refinement statistics. HLA-DR1 (*27*) was cocrystalized with TSST-1 in a 1:1 molar ratio (final total protein concentration of ~12 mg/ml, 10 mM tris buffer, pH 7.5). Crystals of lyophilized TSST-1 (Sigma or Toxin Technology) grown by vapor diffusion from 100 mM acetate (pH 5.5), 17% polyethylene glycol (4 kD), and 5% ethylene glycol (or methyl-propanediol) at room temperature have space group *I*4, with unit cell dimensions of $a = b = 144.08$ Å and $c = 106.55$ Å. Diffraction data to 3.5 Å resolution from a native crystal and from one heavy atom derivative [soaked in 3 mM ethylmercury-thiosalicylate (EMTS) solution for 3 hours] were collected at room temperature with the use of an MAR-research detector with CuKα x-rays generated by an Elliot GX-13 rotating anode with Franks double mirror optics. Data were processed and scaled with the program XDS (*28*). The heavy atom position was determined from difference Patterson maps and was confirmed by difference Fourier analysis with the molecular replacement phases calculated from either the DR1 molecule alone or the TSST-1 molecule alone with the use of the program ROCKS (*29*). The heavy atom binding site is common to that of other DR1 crystal forms (*7, 16*). Heavy atom parameters were refined and single isomorphous replacement (SIR) phases calculated with the program PHARE. SIR phases were improved by solvent flattening (*30*) (50% solvent) to give a 3.5 Å electron density map in which DR1 and TSST-1 were located by a six-dimensional real space search (*17*). DR1 and TSST-1 locations were revealed as peaks nine and five times, respectively, the standard deviation in independent, six-dimensional search functions. DR1 and TSST-1 positions were also independently determined by molecular replacement methods with the use of the program package X-PLOR (*18*). The correlation coefficients calculated for the highest peaks in the DR1 and TSST-1 rotation functions were 0.11 and 0.10, both twofold greater than the next highest peaks. The translation function values were 0.22 and 0.31, respectively, with standard deviations of 0.012. *R* factors calculated from DR1 or TSST-1 alone were 49.7 and 48.6%, respectively. The relative locations of the DR1 and TSST-1 molecules along the crystallographic *z* axis were determined by inspection of the heavy atom binding sites determined by difference Fourier analysis with the use of either DR1 model phases or TSST-1 model phases. The *R* factor for the TSST-1:DR1 complex thus located was 43%. The location of DR1 and TSST-1 determined by molecular replacement and independently by the six-dimensional search of the SIR map were the same, revealing one TSST-1:DR1 complex per asymmetric unit. A further indication that the location of DR1 was correct was the discovery in this crystal of the same dimer of DR1 molecules seen in three earlier crystals containing DR1 (*7, 16*), this time positioned on a crystallographic twofold symmetry axis. f_H, heavy atom structure factor; *E*, residual lack of closure; FOM, mean figure of merit; rms, root mean square.

Data set	Resolution (Å)	Data coverage (%)	R_{merge}* (%)	R_{iso}† (%)	FOM	rms f_H/E
Native	3.5 (3.7 to 3.5)	92.2 (92.8)	10.8 (27.8)			
Derivative	3.5 (3.7 to 3.5)	95.5 (98.3)	12.9 (32.8)	20.0	0.40	1.51

*$R_{merge} = \Sigma_{hkl}\Sigma_{obs} | I^{hkl}_{obs} - \langle I^{hkl} \rangle | / \Sigma_{hkl}\Sigma_{obs} I^{hkl}_{obs}$ where I_{obs} is the observed intensity. †$R_{iso} = \Sigma_{hkl} | F_{native} - F_{derivative} | / \Sigma_{hkl} F_{native}$.

J. Kim and D. C. Wiley, Howard Hughes Medical Institute and Laboratory of Molecular Medicine, Children's Hospital, Boston, MA 02115, USA, and Department of Molecular and Cellular Biology, Harvard University, Cambridge, MA 02138, USA.
R. G. Urban and J. L. Strominger, Department of Molecular and Cellular Biology, Harvard University, Cambridge, MA 02138, USA.
*To whom correspondence should be addressed.

placement, solvent-flattened 3.5 Å electron density map. The same locations were found by independent rotation and translation function calculations (*18*) for each protein in the TSST-1:DR1 crystal (Table 1).

The current model contains 94% of the residues of DR1, 13 alanine residues representing antigenic peptides bound to DR1, and the entire 194 amino acids of TSST-1. (Residue numbers are prefixed with α and β to indicate the α and β subunits of the DR1 molecule, and p and t to indicate the antigenic peptide bound on DR1 and TSST-1, respectively.) The model is presently refined to a crystallographic *R* factor of 0.22 (10 to 3.5 Å, R_{free} = 35%) (Table 2). Because significant intensity data were unmeasurable beyond 3.5 Å resolution, high-resolution details, such as the certainty of hydrogen bonding or salt bridge formation, which require a high-resolution refined structure, cannot be reliably assessed from the current model. However, a series of simulated annealing omit maps calculated around the contact regions clearly shows that the location of side chains and the composition of the interfaces in the TSST-1:DR1 complex are evident. DR1 crystallizes as a dimer of the αβ heterodimer, as has been observed in other DR1 crystal forms (*7*, *16*).

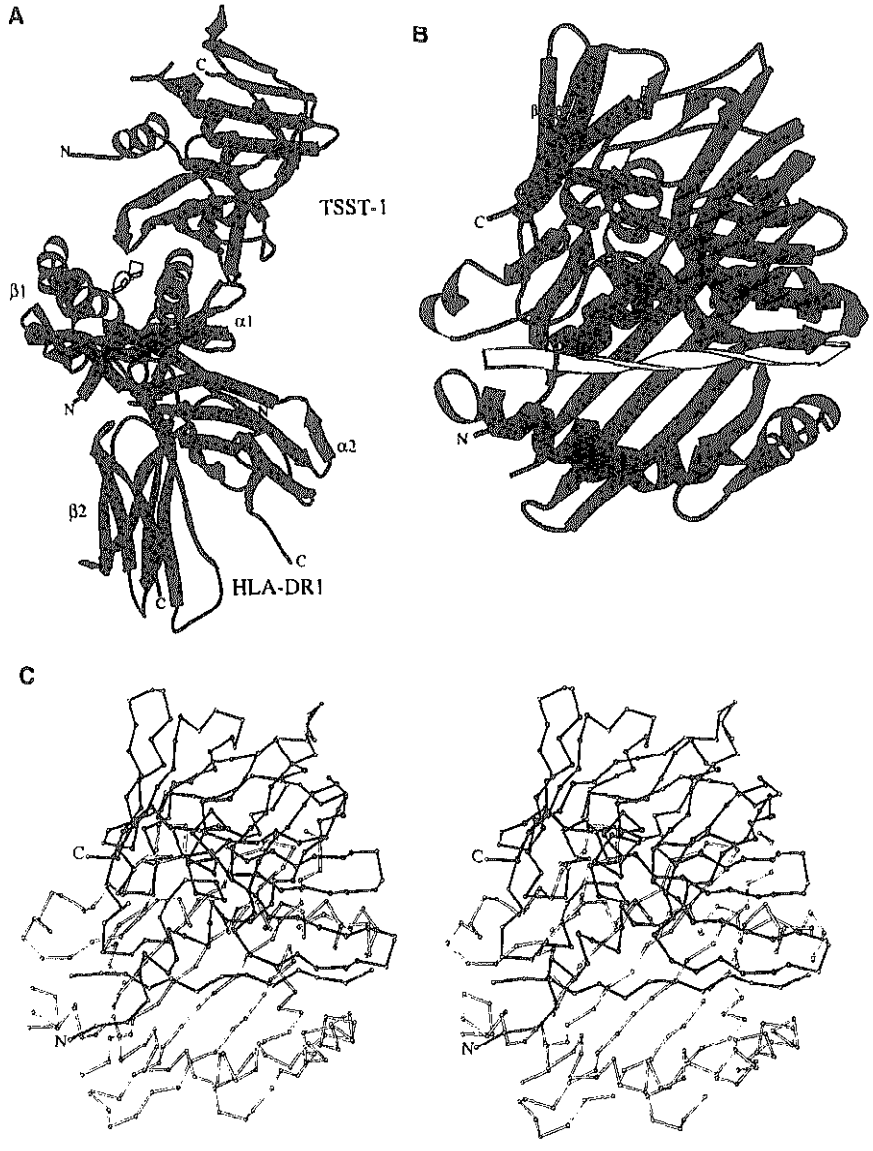

Fig. 1. (**A**) The TSST-1:DR1 complex [all the figures are generated with MolScript (*32*)]. The α and β subunits of DR1 are light blue and blue, respectively, the antigenic peptide is yellow, and TSST-1 is red. (**B**) The TSST-1:DR1 complex viewed toward the MHC peptide binding site of DR1 [coloring is as in (A)]. Secondary structural elements of TSST-1 (α1 and α2 and β1 through β12) are marked for comparison with (C). (**C**) Stereo view of the TSST-1:DR1 complex viewed as in (B). The α1 and β1 domains of DR1 are in white, the antigenic peptide is shaded, and TSST-1 is black. The α2 and β2 domains of DR1 are omitted for clarity. The secondary structural elements of TSST-1 are marked by closed circles for the α carbons: t5 through t14 (α1), t18 through t28 (β1), t32 through t37 (β2), t41 through t47 (β3), t60 through t75 (β4), t79 through t89 (β5), t101 through t106 (β6), t109 through t111 (β7), t119 through t124 (β8), t125 through t140 (α2), t152 through t158 (β9), t162 through t167 (β10), t180 through t182 (β11), and t187 through t193 (β12). C, COOH-terminus; N, NH_2-terminus.

The overall structure of the TSST-1:DR1 complex is shown in Fig. 1. The NH_2-terminal β barrel domain of TSST-1 is primarily involved in complex formation between DR1 and TSST-1 molecules, as had been suggested by x-ray crystallographic analysis of TSST-1 (*9*, *10*) and peptide studies mapping the TSST-1:MHC interaction (*19*). The COOH-terminal domain of TSST-1 is oriented up and away from the DR1 molecule (Fig. 1A). The TSST-1 molecule covers the entire top of the DR1 α1 domain and about half of the peptide binding groove (Fig. 1, B and C).

Although a continuous surface, the TSST-1:DR1 interface (Fig. 2A) can be usefully divided into three major contact regions: an interdigitation of two loops from TSST-1 (near t30 and t50) with two loops from DR1 (near α18 and α38) (contact region I), the packing of four β strands of TSST-1 on the top of the α helix of the α1 domain of DR1 (contact region II), and an interaction between the antigenic peptide bound on DR1 and two β strands from TSST-1 (contact region III). Twenty-four residues of TSST-1 and 20 residues of DR1 (Table 3), making hydrophobic interactions, hydrogen bonds, and salt bridges, form an extensive contact [~1000 $Å^2$ buried with the use of a 1.4 Å solvent probe (*20*)].

Contact region I (Fig. 2B) is centered on Leu^{30} of TSST-1, which is surrounded by nonpolar residues (M36, I63, and Y13) (*21*) of DR1. This leucine is conserved in SEB (L30 of TSST-1 = L45 of SEB) (Table 3) and makes similar contacts to DR1 in the SEB:DR1 interface (*7*). In both the TSST-1:DR1 and SEB:DR1 interfaces, this leucine is one of the most extensively buried residues (159 $Å^2$ in TSST-1; 80 $Å^2$ in SEB). To one side (left, Fig. 2B) of the leucine, polar residues (D27 and K58) of TSST-1 potentially hydrogen bond to polar residues (Q18, Y13, and K67) of DR1. On the other side of the leucine (right, Fig. 2B), K39 of DR1 potentially hydrogen bonds to S53 and the main chain carbonyl oxygen of P50 on TSST-1. In the SEB:DR1 interface, the same DR1 K39 formed a very different contact, forming a salt bridge to SEB E67 (*7*) (Fig. 3). Mutation of DR1 K39 has been shown to disrupt binding of both TSST-1 and SEB (*14*, *15*).

In contact region II, the top face of four turns of the α helix on the DR1 α1 domain (α57 to α71) (Fig. 2C), a site also recognized by T cell receptors, is covered by four

β strands of TSST-1 (β2, β3, β5, and β4) (Fig. 1B). Six of the 10 DR1 residues in the contact (α57, α60, α61, α63, α64, and α67) when mutated affect T cell stimulation by conventional antigens (8). The same six DR1 residues are contacted by SEB, but the contact is made by SEB disulfide loop residues 94 to 97 (7), which are deleted in TSST-1 (replaced by the short loop between β4 and β5) (Fig. 1B). In the TSST-1:DR1 interface, five of the 10 DR1 helical residues are highly conserved in class II MHC sequences and five are polymorphic (22). About 63% of the buried surface in region II is contributed by the conserved DR1 residues, which may be enough to stabilize this contact in TSST-1 complexes with other class II MHC molecules. A cluster of nonpolar residues on the concave surface of the TSST-1 β sheet (I42, L44, I46, P50, I81, and F83) (10) interact with most DR1 α-helical residues; at one end of this interface, the charged DR1 residues E71 and K67 potentially form a salt bridge and hydrogen bond with TSST-1 R34 and the main chain at D27, respectively (Fig. 2C). L46 of TSST-1, which is in the center of the apolar core of contact region II (Fig. 2C), is homologous to E67 of SEB, which in the DR1:SEB complex is connected by a salt bridge to K39 in contact region I of DR1.

In contact region III (Fig. 2D), a β loop of TSST-1 (β4 and β5) makes a few interactions with the COOH-terminal region of the bound peptides and the top of one turn of the β1 domain α helix. Residues 7 to 13 (p7 to p13) of the peptide are near TSST-1 residues K70, Q73, I81, and F83, and residues T75 and S76 appear close enough to hydrogen-bond to p13. Q73 of TSST-1 may hydrogen-bond to DR1 β chain residues Y60 and Q64 (Fig. 2D). Q73 of TSST-1 is homologous to C93 of SEB. In the SEB:DR1 interface, that SEB residue (C93) contacts the top of the α1 domain α helix and thus resides in contact region II rather than in region III, as in TSST-1:DR1.

Although the structures of TSST-1 and SEB are very similar (9, 10), SEB contacts only DR1 at two regions—on one side of DR1 (contact region I) and on top of the α

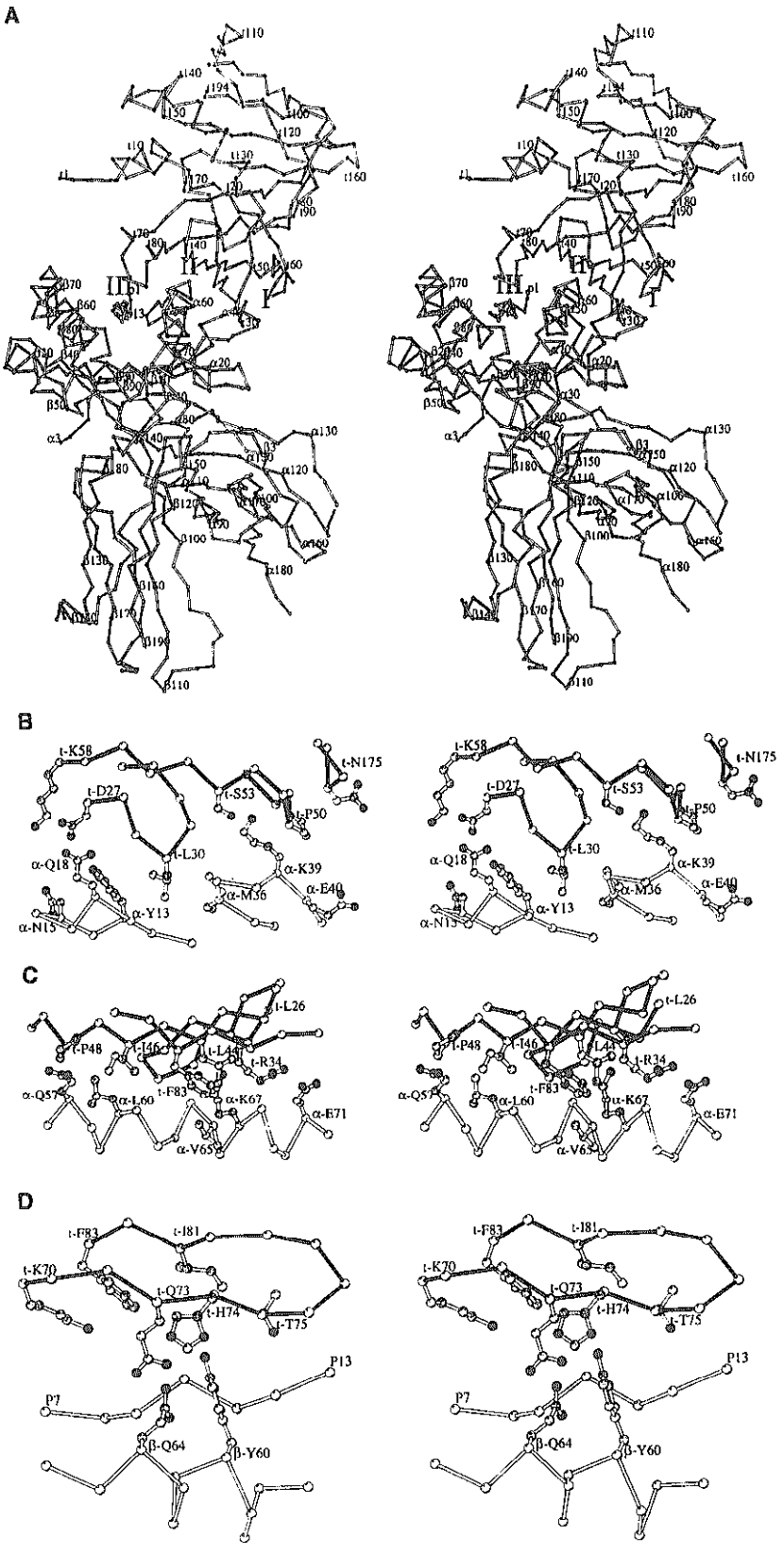

Fig. 2. (**A**) Three major contact regions in TSST-1:DR1 are designated by I, II, and III, respectively (33). The Cα positions of DR1 are indicated by open circles and those of TSST-1 by closed circles. (**B**) Contact region I. The DR1 and TSST-1 Cα chains are indicated by light bonds and dark bonds, respectively. Contact region I is formed by interdigitation of two loops from the DR1 molecule (α13 to α18 and α36 to α39) and two loops from the TSST-1 molecule (t27 to t34 and t42 to t58). Some residues from the COOH-terminal domain of TSST-1 are also located in this region. (**C**) Contact region II. DR1 and TSST-1 Cα chains are indicated by light bonds and dark bonds, respectively. Four β strands from the NH_2-terminal domain of TSST-1 cover the α helix from the α1 domain of DR1. (**D**) Contact region III. DR1 and TSST-1 Cα chains are indicated by light bonds and dark bonds, respectively. TSST-1 interacts with the COOH-terminal region of the antigenic peptide (p7 to p13) and some residues from the β1 domain α helix of DR1.

chain α helix (contact region II)—whereas TSST-1 has one further contact region, to the bound peptide and the DR1 β chain. Both TSST-1 and SEB use homologous leucines (L30 TSST-1 and L45 SEB) to form contact region I, but TSST-1 uses residues (like L46 and F47) that were part of contact region I in SEB:DR1 to form contact region II on top of the DR1 helix, and TSST-1 uses residues (like Q73) that were part of contact region II (top of the α helix) in SEB:DR1 to reach over the top of the peptide and β chain to form contact region III.

Structural models for the interaction of TCRs with superantigens have been proposed on the basis of mutation studies and the three-dimensional structures of SEB, TSST-1, and the SEB:DR1 complex (*7*, *10*). Sites on TSST-1 where mutations affect TCR binding (Fig. 3) form a surface facing up away from the DR1 molecule in the TSST-1:DR1 complex. The very different mode of binding of TSST-1 to class II MHC molecules seen here, relative to SEB, suggests that TCRs may be oriented very differently in complexes with various superantigens (*23*), yet still may be capable of initiating a signal solely on the basis of crosslinking MHC-bearing membranes to TCR-bearing membranes. Although the structures of the complexes of SEB and TSST-1 with DR1 both suggest that TCRs could simultaneously contact superantigen and DR1 molecules, the TSST-1:DR1 complex also suggests the possibility that TCRs might contact only TSST-1 and be blocked from contacting DR1.

The binding of TSST-1 to class II MHC molecules is known to be affected by changes in the α1 and β1 domains of DR molecules (*14*, *24*) and to mutations at residues α36 and α39 (*14*, *25*), which is consistent with the interface observed in the TSST-1:DR1 crystals (Figs. 1 and 2). A comparison of the structure of the TSST-1:DR1 complex with that of the SEB:DR1 complex (*7*)

Table 2. Refinement statistics. TOM/FRODO (*31*) was used for model building, and X-PLOR (*18*) was used in the refinement with PARAM19X.PRO as the parameter file. Four refinement steps were carried out with the available 3.5 Å resolution data. The initial molecular replacement model refined as rigid molecules had a value for R_{cryst} of 43%. Residues in poor electron density in the map calculated from combined SIR and model phases were eliminated from the model. Cycles of positional and individual *B* factor least squares refinement reduced the *R* factor to 25% and R_{free} to 38%. Improvements in phases allowed the omitted residues to be rebuilt from inspection of $2F_o - F_c$ and $F_o - F_c$ electron density maps. After rebuilding, a simulated annealing (3000°) and individual *B* factor refinement reduced the value for R_{cryst} to 22%. Although the value for R_{free} did not drop significantly at this stage, significant improvement of electron density was observed. After rebuilding into the resultant $2F_o - F_c$ map, the initial *R* factor was 38%, and subsequent positional and individual *B* factor refinement reduced the *R* factor to 22% and R_{free} to 35%. As a precaution against model bias in placing side chains, a series of simulated annealing omit maps (*18*) was examined. The absence of intensity data beyond 3.5 Å resolution limits the effectiveness of this refinement, so that the precision of atomic positions and the certainty of side chain placement is reduced. R_{free} was calculated with ~10% of reflections excluded from the refinement. The number of reflections in the refinement was 10,546 (with $F_{obs} > 0$); the number of reflections in the free set was 1050; the number of atoms in the refinement was 4654; and the number of solvent molecules was 0.

Structural statistics	Before refinement	After partial refinement
R_{cryst}* (10.0 to 3.5 Å)	0.38	0.22
R_{free}* (10.0 to 3.5 Å)	0.38	0.35
Root mean square deviation		
Bond lengths (Å)	0.02	0.018
Bond angles (degrees)	2.7	3.5
Dihedral angles (degrees)	31.0	27.0
Improper torsion (degrees)	1.6	1.5

*R_{cryst} and $R_{free} = \Sigma_{hkl} \| F_{obs} \| - \| F_{calc} \| / \Sigma_{hkl} | F_{obs} |$, where F_{obs} is the observed structure factor.

Table 3. The TSST-1:DR1 interface. Underlined residue numbers are also found in the DR1:SEB interface.

TSST-1 residue (SEB residue no.) [buried surface area (Å²)]	Location	DR1 contact residues* [buried surface area (Å²)]
t-D27† (D42) (35.8)	β1	α-Q18 (79.4); α-Y13† (13.8); α-K67† (93.5)
t-S29 (F44) (29.8)	β1β2 loop	
t-L30 (L45) (156.9)	β1β2 loop	α-M36 (45.0); α-I63 (19.7)
t-G31 (Y46) (34.2)	β1β2 loop	
t-S32 (F47) (31.0)	β2	α-A64 (54.2)
t-R34‡ (L49) (93.9)	β2	α-E71‡ (51.5); α-A68 (41.3)
t-I42 (N63) (11.5)	β3	
t-L44 (R65) (49.0)	β3	
t-I46 (E67) (74.3)	β3	α-A61 (26.7); α-Q57 (85.1)
t-F47† (F68) (15.2)	β3	α-K39† (120.4)
t-P48 (K69) (60.9)	β3β4 loop	α-L60 (53.1)
t-P50 (K71) (68.4)	β3β4 loop	α-K39 (120.4); α-K38 (38.5)
t-S53† (A74) (25.4)	β3β4 loop	α-K39† (120.4)
t-K58† (–) (17.8)	β3β4 loop	α-Q18† (79.4)
t-T69 (Y89) (10.1)	β4	
t-K70 (Y90) (39.6)	β4	
t-Q73† (C93) (78.3)	β4	β-Y60† (57.3); β-B64† (37.8)
t-H74 (T94) (36.6)	β4	
t-T75† (F95) (54.5)	β4	p-A13† (61.6)
t-S76† (S96) (14.7)	β4β5 loop	p-A13† (61.6)
t-E77 (K97) (21.7)	β4β5 loop	
t-I81 (K111) (21.5)	β5	
t-F83 (C113) (15.3)	β5	α-V65 (37.3)
t-I85 (Y115) (12.8)	β5	
Other residues at the contact region with more than 4 Å separation from the TSST-1 residues		α-I72 (25.2) p-A7 (13.6) p-A10 (45.8)

*van der Waals contact (< ~3.8 Å). †Potential hydrogen bond (< ~3.5 Å). ‡Potential salt bridge.

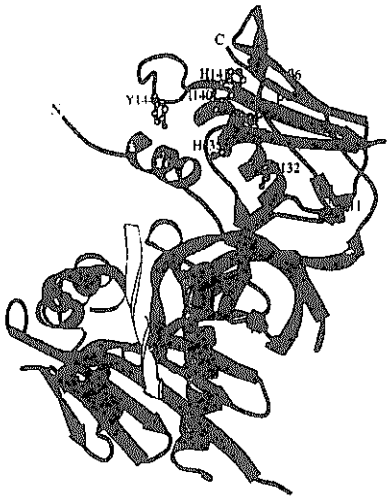

Fig. 3. Location of TSST-1 residues reported to be involved in TCR interactions. The α1 and β1 domains of DR1 are in light blue and blue, the antigenic peptide is yellow, and TSST-1 is red. Residues t-Y115, t-E132, t-H135, t-I140, t-H141, and t-Y144, which are important for mitogenic activity of TSST-1 (*26*) and have been implicated in TCR binding (*9*, *10*), are represented as ball-and-stick models.

reveals that 11 of the 17 DR1 residues in the TSST-1:DR1 interface (underlined in Table 3) are common to the SEB:DR1 interface, despite the overall difference in orientations of the two superantigens on DR1. (Thirteen of the 19 positions on TSST-1 that contact DR1 are homologous to positions on SEB that contact DR1.) Thus, it seems impossible for TSST-1 and SEB to bind simultaneously to DR1, as they would need to occupy the same space. Yet, neither TSST-1 nor SEB appears to be able to completely inhibit the binding of the other (*11*, *13*, *25*). One possible explanation for this dilemma would be the existence of a second binding site on DR1 for SEB or TSST-1, but there is no evidence for such a site.

The most striking new observation about superantigen–class II interaction seen in the TSST-1:DR1 complex is that the superantigen covers most of the peptide binding site, contacting all the polymorphic residues on the α chain α helix, residues on the bound peptide, and part of the β chain α helix, across the peptide binding site. This contrasts with our expectation because superantigen activation of T cells is reportedly much less MHC-restricted and peptide-dependent than peptide antigen–induced activation. It suggests that TSST-1 binding to DR1 may be in part peptide-dependent. Recent binding measurements between superantigens and DR molecules on different cell types suggest that different subsets of HLA-DR molecules may bind TSST-1 and SEB (*25*). Peptide-dependent binding offers a possible mechanism for superantigens to distinguish different subsets of DR1 molecules and that in turn could account for the inability of TSST-1 to inhibit completely the binding of SEB to DR1. Superantigen activation dependent on peptide (and hence also MHC allele) would allow a pathogen to direct T cell activation by its antigens or by host antigens during infections, with potential consequences for inducing specific autoreactivity.

REFERENCES AND NOTES

1. P. Marrack, M. Blackman, E. Kushnir, J. Kappler, *J. Exp. Med.* **171**, 455 (1990).
2. Y. Choi *et al.*, *ibid.* **172**, 981 (1990).
3. B. Fleischer and H. Schrezenmeier, *ibid.* **167**, 1697 (1988); P. Marrack and J. Kappler, *Science* **248**, 705 (1990).
4. A. M. Pullen, J. Bill, R. T. Kubo, P. Marrack, J. W. Kappler, *J. Exp. Med.* **173**, 1183 (1991); B. Fleischer and H.-W. Mittrücker, *Eur. J. Immunol.* **21**, 1331 (1991); A. Seth *et al.*, *Nature* **369**, 324 (1994).
5. R. M. Germain and D. H. Margulies, *Annu. Rev. Immunol.* **11**, 403 (1993).
6. A. M. Pullen, T. Wade, P. Marrack, J. W. Kappler, *Cell* **61**, 1365 (1990); Y. Choi *et al.*, *Nature* **346**, 471 (1990).
7. T. S. Jardetzky *et al.*, *Nature* **368**, 711 (1994).
8. P. Dellabona *et al.*, *Cell* **62**, 1115 (1990); J. L. Jorgensen, P. A. Reay, E. W. Ehrich, M. M. Davis, *Annu. Rev. Immunol.* **10**, 835 (1992).
9. G. S. Prasad *et al.*, *Biochemistry* **32**, 13761 (1993).
10. K. R. Acharya *et al.*, *Nature* **367**, 94 (1994); S. Swaminathan, W. Furey, J. Pletcher, M. Sax, *ibid.* **359**, 801 (1992).
11. P. R. Scholl, A. Diez, R. S. Geha, *J. Immunol.* **143**, 2583 (1989).
12. J. D. Fraser, *Nature* **339**, 221 (1989).
13. M. M. Chintagumpala, J. A. Mollick, R. R. Rich, *J. Immunol.* **147**, 3876 (1991).
14. P. Panina-Bordignon, X.-t. Fu, A. Lanzavecchia, R. W. Karr, *J. Exp. Med.* **176**, 1779 (1992).
15. J. Thibodeau, N. Labrecque, F. Denis, B. Huber, R.-P. Sékaly, *ibid.* **179**, 1029 (1994).
16. J. H. Brown *et al.*, *Nature* **364**, 33 (1993); L. J. Stern *et al.*, *ibid.* **368**, 215 (1994).
17. P. J. Bjorkman *et al.*, *ibid.* **329**, 506 (1987); M. A. Saper, P. J. Bjorkman, D. C. Wiley, *J. Mol. Biol.* **219**, 277 (1991).
18. A. T. Brünger, *J. Mol. Biol.* **203**, 803 (1988).
19. C. Edwin *et al.*, *J. Infect. Dis.* **163**, 524 (1991); J. M. Soos, J. K. Russell, M. A. Jarpe, C. H. Pontzer, H. M. Johnson, *Biochem. Biophys. Res. Commun.* **191**, 1211 (1993).
20. B. Lee and F. M. Richard, *J. Mol. Biol.* **55**, 379 (1971).
21. Abbreviations for the amino acid residues are as follows: A, Ala; C, Cys; D, Asp; E, Glu; F, Phe; G, Gly; H, His; I, Ile; K, Lys; L, Leu; M, Met; N, Asn; P, Pro; Q, Gln; R, Arg; S, Ser; T, Thr; V, Val; W, Trp; and Y, Tyr.
22. J. H. Brown *et al.*, *Nature* **332**, 845 (1988).
23. K. R. Hudson, S. C. Lowe, R. G. Urban, J. D. Fraser, personal communication.
24. D. R. Karp, C. L. Teletski, P. Scholl, R. Geha, E. O. Long, *Nature* **346**, 474 (1990); N. S. Braunstein, D. A. Weber, X. C. Wang, E. O. Long, D. Karp, *J. Exp. Med.* **175**, 1301 (1992).
25. J. Thibodeau *et al.*, *Science* **266**, 1874 (1994).
26. L. Blanco *et al.*, *Infect. Immun.* **58**, 3020 (1990); P. F. Bonventre, H. Heeg, C. Cullen, C. J. Lian, *ibid.* **61**, 793 (1993); D. L. Murray *et al.*, abstract, 93rd General Meeting of the American Society of Microbiology (Atlanta, GA, 1993), vol. 64.
27. J. C. Gorga, V. Horejsi, D. R. Johnson, R. Raghupathy, J. L. Strominger, *J. Biol. Chem.* **262**, 16087 (1987). Water-soluble human lymphocyte antigen–DR1 (HLA-DR1) molecules (DRA and DRB1*0101) were immunoaffinity-purified from the lymphoblastoid cell line LG-2 and digested with papain in a manner similar to that described by Gorga *et al.* (above). Detergent-soluble DR (10 mg) was digested with papain, and after iodoacetamide quenching the DR1-papain mixture was dialyzed 12 hours at 4°C against 50 volumes of deionized water. The dialyzed mixture was then transferred to pre-chilled ultracentrifugation tubes and subjected to 35,000*g* for 1 hour at 4°C. The cleared supernatants were then adjusted to 50 ml containing a 2% final concentration of ampholytes (Ampholine, 3.5-10, Pharmacia LKB, Uppsala, Sweden). The mixture was then transferred into a preparative isoelectric focusing cell (Rotofor, Bio-Rad Laboratories, Richmond, CA) and focused at 12 W for 5 hours at 4°C. Fractions were then collected, and those containing DR (pH 4.0 to 5.5) were pooled and dialyzed against 50 volumes of 10 mM tris-HCl (pH 7.5). The sample was then concentrated to 2 ml by vacuum dialysis against 10 mM tris-HCl (pH 7.5) and further purified by size exclusion chromatography (SEC-3000; 5 μm; 7.5 cm by 30 cm, Beckman Instruments). The DR peak was collected and reconcentrated to >10 mg/ml by vacuum dialysis as above.
28. W. Kabsch, *J. Appl. Crystallogr.* **21**, 916 (1988).
29. G. N. Reeke, *ibid.* **17**, 125 (1984); D. H. Bethe, *ibid.*, p. 215.
30. B. C. Wang, *Methods Enzymol.* **115**, 90 (1985).
31. T. A. Jones, *ibid.*, p. 151.
32. J. P. Kraulis, *J. Appl. Crystallogr.* **24**, 946 (1991).
33. Another contact is found in the crystal between a symmetrically related *TSST-1 molecule and the TSST-1:DR1 complex. Of the six TSST-1 residues implicated in TCR recognition by mutagenesis (Y115, E132, H135, I140, H141, and Y144) (*26*), two (Y115 and Y144) are in the TSST-1:*TSST-1 contact and three (H135, I140, and H141) are in its immediate vicinity.

34. We thank D. H. Ohlendorf, J. H. Brown, and L. J. Stern for the coordinates of TSST-1 and DR1; N. Ramesh and R. S. Geha for an initial sample of purified TSST-1; P. Klimovitsky and A. Haykov for technical assistance; and M. Pietras for large-scale production of tissue culture cells. Discussions with T. S. Jardetzky, D. N. Garboczi, and A. Seth and help from D. C. Rees, P. J. Bjorkman, S. E. Ryu, M. J. Eck, R. S. Brown, R. Nolte, and C. Garnett are appreciated. J.K. acknowledges support by the Howard Hughes Medical Institute (HHMI) and NIH. R.G.U. is supported by the Irvington Institute for Medical Research. D.C.W. is an investigator of HHMI. Research supported by an NIH grant to D.C.W. Coordinates will be deposited in the Protein Data Bank and are available before their release by e-mail (kim@xtal0.harvard.edu).

11 July 1994; accepted 19 October 1994